VNUHCM Journal of Science and Technology Development 2026, 29(3):4283-4290
Open Access Full Text Article

Research Article

New $(g-2)_\mu$ Data and LFV Decays in a Left-Right Model

Nguyen Hua Thanh Nha[1,2,3,4], Le Tho Hue[3,4], Lam Thi Thanh Phuong[2,5,6], Hong Thi Trinh[2,6,*]

Use your smartphone to scan this QR code and download this article

ABSTRACT

Lepton-flavor-violating (LFV) processes involving charged leptons, such as $e_b \to e_a \gamma$, the Standard Model (SM)-like Higgs boson decays $h \to e_b^+ e_a^-$, and the neutral gauge boson decays $Z \to e_b^+ e_a^-$, are beyond the SM framework. Nevertheless, these processes remain among the primary targets of current and future experimental searches. Consequently, extensions of the SM, including our recently proposed left-right (LR) symmetric model with inverse seesaw neutrinos, are required to simultaneously investigate LFV decays and sizable anomalous magnetic moments (AMMs) of charged leptons consistent with experimental observations.

Experimental data on these quantities $a_{e_a} \equiv \frac{(g-2)_{e_a}}{2}$, often significantly affect the phenomenologically viable regions that predict LFV decay rates, particularly in beyond the standard model (BSM) scenarios that also account for neutrino oscillation data.

It is therefore essential to analyze a_{e_a} together with the aforementioned decays within the allowed regions of the parameter space of such models in order to assess the potential of future experimental LFV searches as promising new physics signals. In this work, we investigate an extension of the LR symmetry model with inverse seesaw neutrinos and numerically demonstrate that the three processes $e_b \to e_a \gamma$, $h \to e_b^\pm e_a^\mp$, and $Z \to e_b^\pm e_a^\mp$ remain promising probes of new physics in light of the 2025 results for the muon AMMs $(g-2)_\mu$. Although this new experimental result is consistent with SM predictions and differs significantly from previous discussions, these decay channels remain potentially testable in near-future experiments, even within parameter regions that allow sizable deviations from the SM predictions for both $(g-2)_{e,\mu}$. Our findings suggest that the allowed regions predicted by the model under consideration are significantly affected by updated experimental upper limits on LFV processes. In addition, several phenomenologically interesting correlations among these observables are identified and discussed in detail.

Key words: left-right symmetric model, lepton-flavor-violating decays, Higgs boson, neutrino oscillation, anomalous magnetic moment.

1Department of Theoretical Physics, Faculty of Physics and Engineering Physics, University of Science, Ho Chi Minh City, Vietnam

[2]Vietnam National University, Ho Chi Minh City, Vietnam

[3]Subatomic Physics Research Group, Science and Technology Advanced Institute, Van Lang University, Ho Chi Minh City, Vietnam

[4]Faculty of Applied Technology, Van Lang School of Technology, Van Lang University, Ho Chi Minh City, Vietnam

[5]Can Tho University, Can Tho City, Vietnam

[6]An Giang University, An Giang, Vietnam

Correspondence

Hong Thi Trinh, An Giang University, An Giang, Vietnam

Email: tthong@agu.edu.vn

History

- Received: 31-12-2025
- Revised: 10-05-2026
- Accepted: 28-05-2026
- Published Online: 28-09-2026

DOI:
https://doi.org/10.32508/vnuhcmj-std.v29i3.4648

Check for updates

Copyright

© VNUHCM Journal . This is an open-access article distributed under theterms of the Creative CommonsAttribution 4.0 International license.

INTRODUCTION

The Standard Model (SM) of particle physics is widely regarded as one of the most successful frameworks in high-energy physics. It not only provides a coherent description of the known particle flavors within each sector, but also organizes them according to well-defined mathematical principles. Despite its remarkable success, however, the SM remains incomplete, as it fails to account for several observed phenomena. One of its major limitations is its inability to explain the experimental evidence for active neutrino oscillations, which are widely considered the first indication of lepton-flavor-violating (LFV) sources. Such phenomena may give rise to sizable LFV decay signals, as predicted in various models beyond the Standard Model (BSM), including scenarios with inverse seesaw (ISS) neutrinos. In particular, the LFV decay processes of charged leptons $e_b \to e_a \gamma$, the SM-like Higgs boson (LFVh) $h \to e_b^\pm e_a^\mp$, and the Z boson (LFVZ) $Z \to e_b^\pm e_a^\mp$ are among the primary targets of current and future experimental searches.[1,2,3,4,5,6]

In addition, experimental constraints from charged-lepton anomalous magnetic moments (AMMs), $a_{e_a} \equiv \frac{(g-2)_{e_a}}{2}$, provide important information regarding the viable regions of the model parameter space that can accommodate sizable LFV decay rates, especially in BSMs with ISS neutrinos, where one-loop contributions affect both classes of observables. Consequently, a combined analysis of these observables within the allowed regions of the parameter space is essential. Consequently, the primary objective of this research is to perform a detailed reanalysis of the correlations between LFV decay rates and the AMMs of the muon and the electron based on our recently published work on the left-right

model with ISS neutrinos (LRIS)[7], as well as the most recent $(g-2)_\mu$ result published in 2025.[8,9] We further present new predictions that differ significantly from those reported in previous studies. The relevant decay rates are constrained by recent experimental bounds as follows[10]:

- For cLFV decays: $Br(\mu \to e\gamma) < 3.1\times10^{-13}$, $Br(\tau \to e\gamma) < 3.3\times10^{-8}$, and $Br(\tau \to \mu\gamma) < 4.2\times10^{-8}$.
- For LFVh decays: $Br(h \to \tau\mu) < 1.5\times10^{-3}$, $Br(h \to \tau e) < 2.0\times10^{-3}$, and $Br(h \to \mu e) < 4.4\times10^{-5}$.
- The LFVZ decays: $Br(Z \to \tau^{\pm}\mu^{\mp}) < 6.5\times10^{-6}$, $Br(Z \to \tau^{\pm}e^{\mp}) < 5.0\times10^{-6}$, and $Br(Z \to \mu^{\pm}e^{\mp}) < 2.62\times10^{-7}$.

The remainder of this paper is organized as follows. The section reviewing the LRIS model summarizes its main features and presents the Feynman rules relevant to LFV processes. In the following section, previously established analytical results[7] are used to investigate the phenomenologically viable regions of the parameter space that are consistent with neutrino oscillation data, LFV constraints, and the most recent measurement of $(g-2)_\mu$ within 1σ of the SM prediction. Finally, in the concluding section, the findings are summarized and their phenomenological implications discussed in light of the results obtained within the LRIS framework.

METHODS

In this work, we adopt a quantum field–theoretical framework and employ the Mathematica software with the LoopTools package to perform numerical investigations within the LRIS model. The detailed derivation and analytical results were established in our previous work[7]; here we briefly summarize the key elements for completeness consistency. The one-loop contributions to the decay amplitudes of cLFV processes, $(g-2)_{e,\mu}$, LFVZ, and LFVh were calculated analytically in the unitary gauge and subsequently cross-checked using the FORM package.[11] We use the previously derived analytical amplitudes,[7] in which the contributions from all relevant Feynman diagrams are expressed in terms of the 1-, 2-, and 3-point Passarino-Veltman functions available in LoopTools. The total amplitudes for all LFV decays were analytically shown to be ultraviolet (UV) finite despite the presence of divergent terms in many intermediate expressions associated with individual Feynman diagrams. The cancellation of UV divergences was also verified numerically.

The general analytical expressions for the loop contributions were derived in the unitary gauge based on the complete sets of Feynman diagrams shown in Fig. 1.

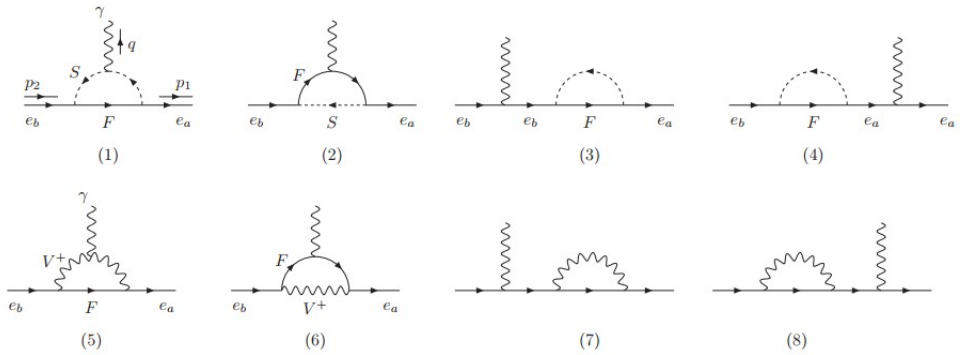

Figure 1: One-loop Feynman diagrams contributing to the cLFV decay amplitudes and AMMs in the unitary gauge, where F, S, and V represents the relevant fermions, Higgs, and gauge boson exchanges, respectively.

Within the LRIS framework, the loop contributions to the charged-lepton AMMs and the corresponding LFV decay amplitudes are expressed in terms of the following form factors:

$$C^{LRIS}_{(ab)R} = C_{(ab)R}(H^+) + C_{(ab)R}(W) + C_{(ab)R}(W'), \quad (1)$$

where H^+, and W' represent singly charged Higgs and gauge bosons, and W represents the SM gauge boson. The respective formulas of AMM and cLFV decay rates are given by[7]:

$$a^{LRIS}_{e_a} = -\frac{4m_a}{e}\mathrm{Re}\left[C^{LRIS}_{(aa)R}\right] - a^{SM}_{e_a}(W),$$

$$Br(e_b \to e_a\gamma)^{LRIS} = \frac{48\pi^2}{G_F^2 m_b^2}\left(|C^{LRIS}_{(ab)R}|^2 + |C^{LRIS}_{(ba)R}|^2\right)Br(e_b \to e_a\bar{\nu}_a\nu_b), \quad (2)$$

where $a^{SM}_{e_a}(W)$ arise from the W boson exchange within the SM framework.

The effective amplitude for LFVZ decays was introduced in detail in previous work[7]; consequently, it is omitted here. In the unitary gauge, the complete set of one-loop Feynman diagrams contributing to the LFVZ decay amplitudes is presented in Fig. 2.

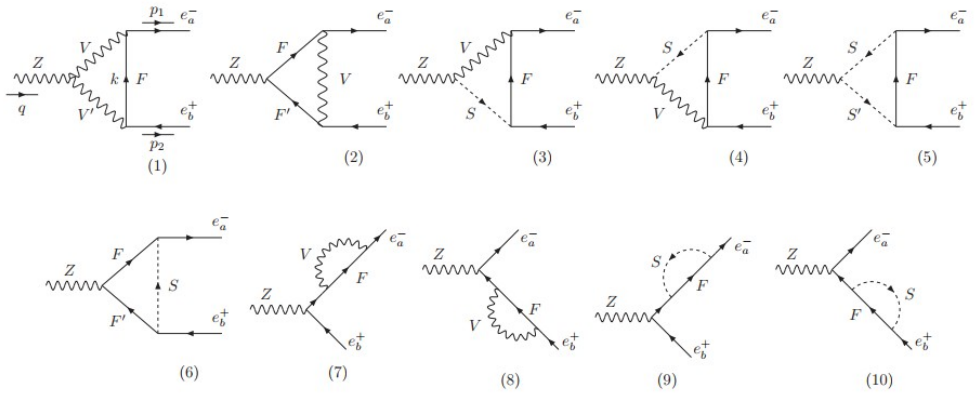

Figure 2: One-loop Feynman diagrams contributing to the LFVZ decay amplitudes and AMMs in the unitary gauge. Here, F and F' denote fermions, while S and V, V' correspond to Higgs and gauge bosons, respectively.

The effective Lagrangian of the LFVh decay and the corresponding partial decay width have been introduced in previous studies.[7,12] The relevant one-loop Feynman diagrams required to evaluate all one-loop contributions in the unitary gauge are displayed in Fig. 3.

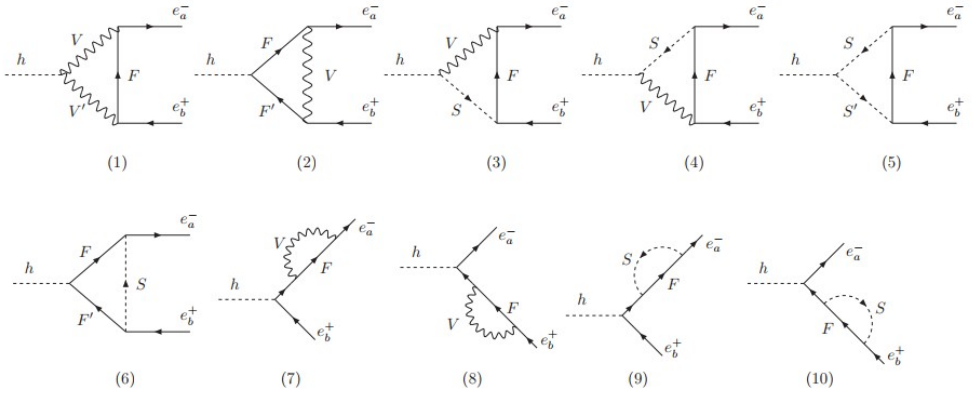

Figure 3: One-loop Feynman diagrams contributing to the LFVh decay amplitudes in the unitary gauge.

Based on the general one-loop Feynman diagrams discussed above, the corresponding Feynman rules and coupling conventions required for the evaluation of the one-loop contributions to specific diagrams were presented in detail previously.[7] Subsequently, the general analytical expressions associated with all relevant one-loop Feynman diagrams were derived in the unitary gauge. For the implementation of a specific model, such as the LRIS model considered in this work, it is first necessary to determine the physical spectrum of the model, particularly those associated with the LFV couplings arising from the exchanges of F, F', S, and V. The couplings of h and Z bosons generating the one-loop diagrams presented in Figs. 2 and 3 are then computed. Finally, complete analytical expressions related to cLFV and LFVh/Z decay amplitudes are obtained and used for subsequent numerical investigations.[7]

BRIEF REVIEW OF THE LRIS MODEL

The left-right (LR) symmetric extension of the SM, defined by the gauge symmetry $SU(3)_c \times SU(2)_L \times SU(2)_R \times U(1)_{B-L}$, has attracted considerable attention in previous studies[7,12,13]. One example is the minimal LR model,[12] which uses the linear seesaw or minimal seesaw mechanism to generate neutrino masses and mixing. The LRIS model represents an alternative extension of the SM. It is characterized by LR gauge symmetry together with a Z_2 discrete symmetry $SU(3)_c \times SU(2)_L \times SU(2)_R \times U(1)_{B-L} \times Z_2$, in which ISS neutrinos can successfully account for the R_D and R_{D^*} anomalies while simultaneously predicting a relatively light scalar spectrum.[13] For completeness, we briefly review the particle spectrum and the Lagrangian framework relevant to our analysis.

The charge operator is defined as $Q = T_3^L + T_3^R + \frac{B-L}{2} = T_3^L + \frac{Y}{2}$, where $T_{L,R}^3, B, L$ are the generators of the gauge group $SU(2)_{L,R}$, the baryon, and lepton numbers of the $U(1)_{B-L}$ group, respectively. The particle spectrum consists of leptons, quarks, and Higgs bosons that transform as the following multiplets:

$$Q_L = \begin{pmatrix} u \\ d \end{pmatrix}_L \sim \left(3,\ 2,\ 1,\ \frac{1}{3},\ +\right),\ Q_R \sim \begin{pmatrix} u \\ d \end{pmatrix}_R \sim \left(3,\ 1,\ 2,\ \frac{1}{3},\ +\right),$$

$$L_L = \begin{pmatrix} \nu \\ e \end{pmatrix}_L \sim (1,\ 2,\ 1,\ -1,\ +),\ L_R = \begin{pmatrix} \nu \\ e \end{pmatrix}_R \sim (1,\ 1,\ 2,\ -1,\ +),$$

$$S_1 \sim (1,\ 1,\ 1,\ 0,\ -),\ S_2 \sim (1,\ 1,\ 1,\ 0,\ +),$$

$$\phi = \begin{pmatrix} \phi_1^0 & \phi_1^+ \\ \phi_2^- & \phi_2^0 \end{pmatrix} \sim (1,\ 2,\ 2,\ 0,\ +),\ \chi_R = \begin{pmatrix} \chi_R^+ \\ \chi_R^0 \end{pmatrix} \sim (1,\ 1,\ 2,\ 1,\ +),$$

where the non-zero vacuum expectation values (VEVs) are $\langle \phi \rangle = diag\left(\frac{v_1}{\sqrt{2}}, \frac{v_2}{\sqrt{2}}\right)$, and $\langle \chi_R^0 \rangle = \frac{v_R}{\sqrt{2}}$. The parameter $t_\beta = \frac{v_1}{v_2}$, and $v^2 = v_1^2 + v_2^2 = (246\ \text{GeV})^2$ are used when matching with the SM.

The above particle spectra are used to construct the Yukawa sectors of quarks and leptons, the Higgs potential, and covariant kinetic Lagrangians of all fermions, Higgs, and gauge bosons. In addition to the physical particles of the SM, the LRIS model predicts several new states that generate significant one-loop contributions to the LFV decay amplitudes and the AMMs of charged leptons. These include nine ISS neutrinos, one singly charged Higgs boson $H^\pm$, and the charged gauge boson $W'^\pm$. In this model, $W_{L,R\mu}^\pm \equiv (W_{L,R\mu}^1 \mp i W_{L,R\mu}^2)/\sqrt{2}$, the $W - W'$ mixing angle, which involves singly charged bosons, is denoted by θ and calculated through the relation $t_{2\theta} = (2 s_{2\beta} v^2)/v_R^2$, leading to the relations $\begin{pmatrix} W_{L\mu}^\pm \\ W_{R\mu}^\pm \end{pmatrix} = \begin{pmatrix} c_\theta & -s_\theta \\ s_\theta & c_\theta \end{pmatrix} \begin{pmatrix} W_\mu^\pm \\ W_\mu'^\pm \end{pmatrix}$, where we examine the simple case in which $g_L = g_R = g_2 = e/s_W$ corresponds to[7] the $SU(2)_L$ SM gauge coupling.

Table 1 summarizes the Feynman rules for SM-like Higgs boson couplings to bosons relevant for LFVh decays[7].

Table 1: SM-like Higgs interaction vertices with charged Higgs and gauge bosons. [Source: Authors']

Vertex	Coupling	Vertex	Coupling
$g_{hW^+W^-}$	$gm_W(1 - s_{2\beta}s_{2\theta})\delta_{hee}^{-1}$	$g_{hW'^+W^-}$	$gm_W(s_{2\beta}s_{2\theta} + 1)\delta_{hee}^{-1}$
$g_{hW^+W'^-}$	$gm_W s_{2\beta}\left(s_\theta^2 - c_\theta^2\right)\delta_{hee}^{-1}$		
$g_{W^+H^-h}$	$\frac{g}{2}c_\xi s_\theta\left(c_\beta^2 - s_\beta^2\right)$	$g_{W'^+H^-h}$	$\frac{g}{2}c_\theta c_\xi\left(c_\beta^2 - s_\beta^2\right)$

We note that Table 1 presents examples of SM-like Higgs couplings with the singly charged Higgs and gauge bosons that generate the one-loop Feynman diagrams shown in Fig. 2. They are derived from the kinetic terms of Higgs boson $L = hV^{+\mu}V^{-\nu}g_{\mu\nu}g_{hVV} + \left(hV^{+\mu}H^- g_{hVV}(p_h - p_H)_\mu + h.c.\right) + \ldots$. Other couplings and parameters of the LRIS model related to cLFV and LFVh/Z decays in our work are consistent with our previous study.[7]

Similarly, representative Feynman rules for the couplings of the Z boson with singly charged Higgs and gauge bosons contributing to the one-loop LFVZ processes $Z \to e_b^+ e_a^-$ are presented in Table 2.[7]

Table 2: Interaction vertices of the Z boson with charged Higgs and gauge bosons. [Source: Authors']

Vertex	Coupling
$g_{ZH^-H^+}$	$-\frac{c_\zeta\left(s_\xi^2 + 2s_W^2 - 1\right)}{2s_W c_W} + \frac{s_\zeta\left(\left(s_\xi^2 + 2\right)s_W^2 - 1\right)}{2s_W c_W\sqrt{1 - 2s_W^2}}$
$\{g_{ZH^-W^+}, g_{ZH^-W'^+}\}$	$\left\{\frac{c_{2\beta}c_\xi m_W s_\theta}{s_W c_W}\left(c_\zeta - \frac{s_\zeta s_W^2}{\sqrt{1 - 2s_W^2}}\right),\ \frac{c_{2\beta}c_\theta c_\xi m_W}{s_W c_W}\left(c_\zeta - \frac{s_\zeta s_W^2}{\sqrt{1 - 2s_W^2}}\right)\right\}$

$\{g_{ZW^+W^-}, g_{ZW^+W^-}\}$	$\left\{\frac{c_\zeta c_\theta^2}{t_W} - s_\theta^2\left(c_\zeta t_W + s_\zeta\sqrt{1-t_W^2}/s_W\right), c_\zeta s_\theta^2 t_W^{-1} - c_\theta^2\left(c_\zeta t_W + s_\zeta\sqrt{1-t_W^2}/s_W\right)\right\}$
$g_{ZW^+W^-}, g_{ZW^+W^-}$	$-c_\theta s_\theta\left(\frac{c_\zeta}{s_W c_W} + s_\zeta\sqrt{1-t_W^2}/s_W\right)$

RESULTS AND DISCUSSION

The numerical values of the experimental inputs are given by[14]:

$$g = 0.652, \alpha_e = \frac{1}{137} = \frac{e^2}{4\pi}, G_F = 1.166\times10^{-5}\,[\text{GeV}^{-2}], s_W^2 = 0.231,$$
$$m_e = 5\times10^{-4}\,[\text{GeV}], m_\mu = 0.105\,[\text{GeV}], m_\tau = 1.776\,[\text{GeV}], \quad (3)$$
$$m_W = 80.377\,[\text{GeV}], m_h = 125.25\,[\text{GeV}], m_Z = 91.1876\,[\text{GeV}], \Gamma_Z = 2.4955\,[\text{GeV}].$$

Here, we concentrate on the best-fit values of the neutrino oscillation data with respect to the normal order (NO) scheme with $m_{n_3} > m_{n_2} > m_{n_1}$ as follows[14]:

$$s_{12}^2 = 0.32, s_{23}^2 = 0.547, s_{13}^2 = 0.0216,$$
$$\Delta m_{21}^2 \equiv m_{n_2}^2 - m_{n_1}^2 = 7.55\times10^{-5}[\text{eV}^2], \quad (4)$$
$$\Delta m_{32}^2 \equiv m_{n_3}^2 - m_{n_2}^2 = 2.424\times10^{-3}[\text{eV}^2].$$

On the other hand, $\delta = 180\,[\text{Deg}]$ is chosen to support large values of Δa_μ while avoiding large electric dipole moments that are excluded by experimental constraints, since $\Delta a_\mu \sim \text{Re}[c_{(aa)R}]$ and $d_{\mu,e} \sim \text{Im}[c_{(aa)R}]$. This choice therefore allows us to efficiently identify the most interesting regions of the parameter space. The neutrino mass spectrum and mixing matrix are fixed as follows:

$$\hat{m}_\nu = \left(\hat{m}_\nu^2\right)^{1/2} = \text{diag}\left(m_{n_1}, \sqrt{m_{n_1}^2 + \Delta m_{21}^2}, \sqrt{m_{n_1}^2 + \Delta m_{21}^2 + \Delta m_{32}^2}\right), \quad (5)$$

$$U_{\text{PMNS}} = f(\theta_{12}, \theta_{13}, \theta_{23}, \delta) = \begin{pmatrix} c_{12}c_{13} & c_{13}s_{12} & s_{13}e^{-i\delta} \\ -c_{23}s_{12} - c_{12}s_{13}s_{23}e^{i\delta} & c_{13}c_{23} - s_{12}s_{13}s_{23}e^{i\delta} & c_{13}s_{23} \\ s_{12}s_{23} - c_{12}c_{23}s_{13}e^{i\delta} & -c_{23}s_{12}e^{i\delta}s_{13} - c_{13}s_{23} & c_{13}c_{23} \end{pmatrix}, \quad (6)$$

where $m_{n_1} \leq 0.035$ eV as constrained by current cosmological observations; this corresponds to an upper bound of $\Sigma m_\nu \leq 0.12$ eV.[15,16]

Experimental data on the $(g-2)_\mu$ AMM reported by the Fermilab collaboration[8,29] indicate a 1σ standard deviation from the SM prediction, given by: $\Delta a_\mu^{\text{new}} \equiv a_\mu^{\text{exp}} - a_\mu^{\text{SM}} = (3.8 \pm 6.3)\times10^{-10}$. In contrast, data derived from a_e experiments conducted by various groups[17,18,19,20] exhibit discrepancies between the results, leading to deviations from the SM prediction in the orders of $|\Delta a_e^{\text{NP}}| = O(10^{-13})$.[21,22,23,24,25,26]

The LFV decay rates discussed above were introduced in the Introduction section, while the remaining model parameters are scanned within the ranges defined below:

$$v_R \in 10 \div 100\,[\text{TeV}], m_{H^\pm} \in 300 \div 5000\,[\text{GeV}], M_{1,2,3} \in 100 \div 10^4\,[\text{GeV}],$$
$$m_{n_1} \in 10^{-3} \div 0.035\,[\text{eV}], t_\beta \in 0.02 \div 0.8, x_0 \in 10^{-6} \div 5\times10^{-4}, (\hat{\mu}_s)_{11,33} \in 0.2 \div 50, \quad (7)$$

The upper bound of $x_0 \equiv \frac{\max[m_{n_1}, m_{n_2}, m_{n_3}]}{|(\mu_s)_{22}|}$ is constrained by experimental limits on the nonunitarity of the active neutrino mixing matrix.[27,28,29] In addition, the three free parameters ξ, which define the Dirac neutrino mass matrix through the Casas-Ibarra parameterization, are scanned over the range $[-\pi,\pi]$.[7] All allowed parameter points obtained in our analysis are required to satisfy both the LFV constraints and the experimental AMM data of the muon and electron.

The numerical correlations between the $|\Delta a_\mu|$ and key parameters v_R, m_{H^+}, and x_0 are presented in Fig. 4. The results show that $|\Delta a_\mu|$ strongly depends on these parameters, reaching values of $O(10^{-9})$, which are consistent with the latest experimental data.[8,9] This behavior is most pronounced in the following parameter ranges: $v_R \in [5,20]$[TeV], $m_{H^+} \in [310,2000]$[GeV], and $x_0 \in [5\times10^{-5}, 5\times10^{-4}]$.

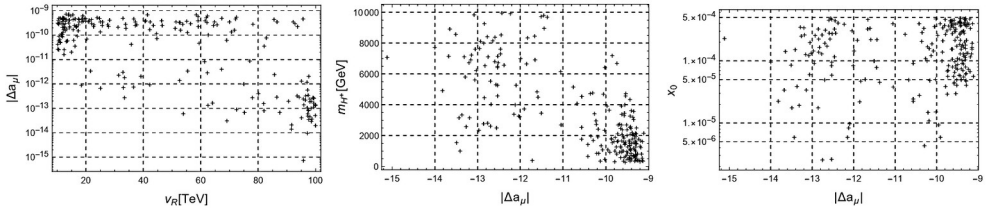

Figure 4: The dependence of $|\Delta a_\mu|$ on parameters in the LRIS model.

The correlations between $|\Delta a_\mu|$ and LFV decay rates are presented in Fig. 5. The predicted rates for the $\tau \to \mu\gamma$, $\mu \to e\gamma$ channels nearly saturate the experimental upper bounds updated in previous studies.[8,9] This result indicates a promising signal for future experimental searches in the channel and differs significantly from the previously reported $O(10^{-13})$ results.[7] In addition, the $Br(\tau \to \mu\gamma)$ is significantly enhanced as the muon AMM increases, approaching the current experimental upper bound when $|\Delta a_\mu|$ reaches its maximal value within the 1σ range of the 2025 data. The two right panels further demonstrate that the LFVh and LFVZ decays are only mildly affected by variations of $|\Delta a_\mu|$.

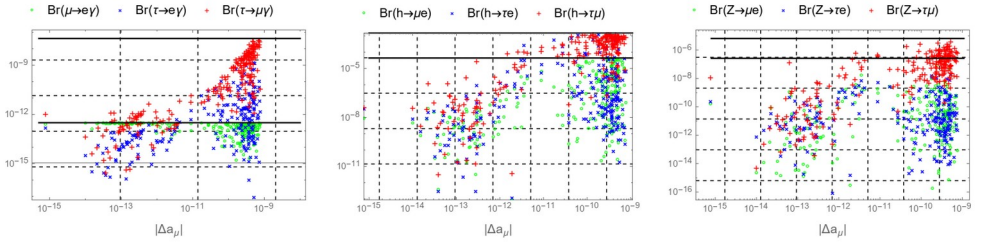

Figure 5: The dependence of LFV decay rates on $|\Delta a_\mu|$. Two black lines in the left, middle, and right panels indicate the upper bounds of LFV decay rates for cLFV $(\tau \to \mu\gamma,\ \mu \to e\gamma)$, LFVh $(h \to \mu\tau,\ h \to \mu e)$, and LFVZ $(Z \to \mu\tau,\ Z \to \mu e)$, respectively.

The correlations of $|\Delta a_e|$ with all LFV decay channels are analyzed numerically and presented in Fig. 6. The numerical results indicate that all LFV decay rates exhibit only a weak dependence on $|\Delta a_e|$. Specifically, $|\Delta a_e|$ can reach values of $O(10^{-13})$, which represents an enhancement compared to the value of $O(10^{-14})$ reported previously.[7]

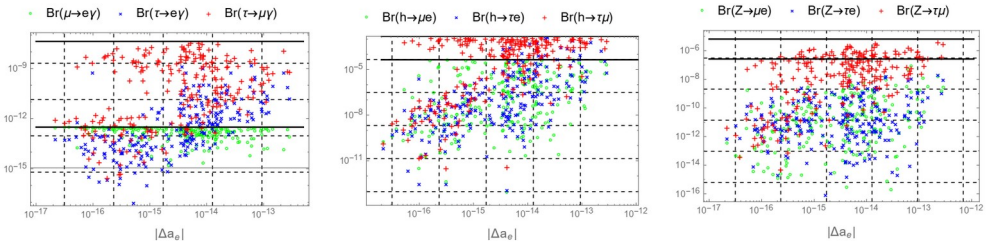

Figure 6: The dependence of LFV decay rates on $|\Delta a_e|$.

Accordingly, our numerical investigations predict the following upper bounds for the LFV decay rates:

- The corresponding bounds for cLFV:

$Br(\mu \to e\gamma) \le 3\times10^{-13}$, $Br(\tau \to e\gamma) \le 2.8\times10^{-9}$, and $Br(\tau \to \mu\gamma) \le 4\times10^{-8}$,

- The corresponding bounds for LFVh:

$Br(h \to \mu e) \le 4.3\times10^{-5}$, $Br(h \to \tau e) \le 8.9\times10^{-5}$, and $Br(h \to \tau\mu) \le 1.3\times10^{-3}$,

- The corresponding bounds for LFVZ:

$Br(Z \to \mu^+e^-) \le 3\times10^{-9}$, $Br(Z \to \tau^+e^-) \le 1.1\times10^{-8}$, and $Br(Z \to \tau^+\mu^-) \le 6\times10^{-6}$.

In contrast to previous work using old $(g-2)_\mu$ data,[7] this work indicates that Δa_e^{LRIS} can reach sizable values of $O(10^{-13})$, consistent with current experimental constraints. The maximal cLFV decay rates depend strongly on $|\Delta a_\mu|$, especially with small $|\Delta a_\mu| < 5\times10^{-10}$. All decay rates can approach the experimental bounds for large $|\Delta a_\mu|$, and can reach values close to the 1σ experimental upper bound of $|\Delta a_\mu| \le 10^{-9}$ as previously reported,[8,9] with the exception of the following:

- The corresponding bounds for cLFV:

$Br(\tau \to e\gamma) \le 2.8\times10^{-9}$, and $Br(h \to \tau e) \le 8.9\times10^{-5}$,

- The corresponding bounds for LFVZ:

$Br(Z \to \mu^+e^-) \le 3\times10^{-9}$, and $Br(Z \to \tau^+e^-) \le 1.1\times10^{-8}$.

Motivated by these results, LFV decay rates $(\mu \to e\gamma, \tau \to \mu\gamma)$, $(h \to \mu e, h \to \tau\mu)$, and $(Z \to \tau^\mp\mu^\mp)$ can all approach the current experimental limits reported by the PDG.[10] Other LFV channels remain within the projected sensitivities of near-future experiments.

CONCLUSIONS

In this study, a new numerical exploration of the correlations between the updated $(g-2)_{e,\mu}$ data and LFV decay rates within the LRIS framework was performed. Notably, it was found that viable regions of the parameter space remain compatible with the most recent experimental bounds from searches for five LFV decays $\mu \to e\gamma$, $\tau \to \mu\gamma$, $h \to \mu e$, $h \to \tau\mu$, and $Z \to \tau^\mp\mu^\mp$, while $(g-2)_{e,\mu}$ is highly sensitive to the available experimental data. Using the most recent 2025 $(g-2)_\mu$ data, our numerical results demonstrate that that many LFV decay channels continue to provide promising new physics signals for future experimental searches. Furthermore, $|\Delta a_e|$ can reach relatively large values of $O(10^{-13})$, consistent with recent experimental constraints.

COMPETING INTERESTS

The authors declare that they have no competing interests.

AUTHORS' CONTRIBUTIONS

Nguyen Hua Thanh Nha contributed to the summary, introduction, the survey of data, and the writing of the draft. Le Tho Hue contributed to the survey of data, and editing of the draft. Lam Thi Thanh Phuong contributed to the brief review of the LRIS model and the calculation of couplings. Hong Thi Trinh contributed to the calculation of couplings, conclusions, and the editing of the draft.

ABBREVIATIONS

BSM: Beyond the Standard Model
SM: Standard Model
LR: left-right symmetric
ISS: inverse seesaw
LFV: lepton flavor violating
PV: Passarino-Veltman
cLFV: LFV decays of the charged leptons
LRIS: LR inverse seesaw
LFVh: LFV decays of the SM-like Higgs boson
LFVZ: LFV decays of the neutral gauge boson
LSS: the linear seesaw
MSS: the minimal seesaw

REFERENCES

1. A. M. Sirunyan *et al.* [CMS], Phys. Rev. D 104 (2021) no.3, 032013 [arXiv:2105.03007 [hep-ex]].
2. [ATLAS], "Search for the decays of the Higgs boson $H \to ee$ and $H \to e\mu$ in pp collisions at $\sqrt{s}$ = 13 TeV with the ATLAS detector," ATLAS-CONF-2019-037
3. A. Hayrapetyan *et al.* [CMS], Phys. Rev. D 108 (2023) no.7, 072004 [arXiv:2305.18106 [hep-ex]].
4. G. Aad *et al.* [ATLAS], JHEP 07 (2023), 166 [arXiv:2302.05225 [hep-ex]].
5. G. Aad *et al.* [ATLAS], Phys. Rev. Lett. 127 (2022), 271801 [arXiv:2105.12491 [hep-ex]].
6. G. Aad *et al.* [ATLAS], Phys. Rev. D 108 (2023), 032015 [arXiv:2204.10783 [hep-ex]].
7. L. T. Hue, K. H. Phan, T. T. Hong, T. P. Nguyen and N. H. T. Nha, Eur. Phys. J. C 84, no.12, 1262 (2024) doi:10.1140/epjc/s10052-024-13624-6 [arXiv:2409.01390 [hep-ph]].
8. M. W. Li, X. G. He, A. Cheek and X. Chu, [arXiv:2506.05511 [hep-ph]].
9. S. Navas *et al.* [Particle Data Group], Phys. Rev. D 110, no.3, 030001 (2024) doi:10.1103/PhysRevD.110.030001

10. P. S. B. Dev, R. N. Mohapatra and Y. Zhang, JHEP 05, 174 (2016) doi:10.1007/JHEP05(2016)174 [arXiv:1602.05947 [hep-ph]].
11. S. Khalil, Phys. Rev. D 82, 077702 (2010) doi:10.1103/PhysRevD.82.077702 [arXiv:1004.0013 [hep-ph]].
12. M. Ashry, K. Ezzat and S. Khalil, Phys. Rev. D 107, no.5, 055044 (2023) doi:10.1103/PhysRevD.107.055044 [arXiv:2207.05828 [hep-ph]].
13. R. L. Workman *et al.* [Particle Data Group], PTEP 2022, 083C01 (2022) doi:10.1093/ptep/ptac097
14. N. Aghanim *et al.* [Planck], Astron. Astrophys. 641 (2020), A6 [erratum: Astron. Astrophys. 652 (2021), C4] [arXiv:1807.06209 [astro-ph.CO]].
15. D. Hanneke, S. Fogwell and G. Gabrielse, Phys. Rev. Lett. 100 (2008), 120801 [arXiv:0801.1134 [physics.atom-ph]].
16. R. H. Parker, C. Yu, W. Zhong, B. Estey and H. Müller, Science 360 (2018), 191 [arXiv:1812.04130 [physics.atom-ph]].
17. L. Morel, Z. Yao, P. Cladé and S. Guellati-Khélifa, Nature 588 (2020) no.7836, 61-65.
18. X. Fan, T. G. Myers, B. A. D. Sukra and G. Gabrielse, Phys. Rev. Lett. 130 (2023) no.7, 071801 [arXiv:2209.13084 [physics.atom-ph]].
19. T. Aoyama, M. Hayakawa, T. Kinoshita and M. Nio, Phys. Rev. Lett. 109 (2012), 111807 [arXiv:1205.5368 [hep-ph]].
20. S. Laporta, Phys. Lett. B 772 (2017), 232-238 [arXiv:1704.06996 [hep-ph]].
21. T. Aoyama, T. Kinoshita and M. Nio, Phys. Rev. D 97 (2018) no.3, 036001 [arXiv:1712.06060 [hep-ph]].
22. H. Terazawa, Nonlin. Phenom. Complex Syst. 21 (2018) no.3, 268-272
23. S. Volkov, Phys. Rev. D 100 (2019) no.9, 096004 [arXiv:1909.08015 [hep-ph]].
24. A. Gérardin, Eur. Phys. J. A 57 (2021) no.4, 116 [arXiv:2012.03931 [hep-lat]].
25. E. Fernandez-Martinez, J. Hernandez-Garcia and J. Lopez-Pavon, JHEP 08 (2016), 033 [arXiv:1605.08774 [hep-ph]].
26. N. R. Agostinho, G. C. Branco, P. M. F. Pereira, M. N. Rebelo and J. I. Silva-Marcos, Eur. Phys. J. C 78 (2018) no.11, 895 [arXiv:1711.06229 [hep-ph]].
27. M. Blennow, E. Fernández-Martínez, J. Hernández-García, J. López-Pavón, X. Marcano and D. Naredo-Tuero, JHEP 08 (2023), 030 [arXiv:2306.01040 [hep-ph]].